geoconvention
Calgary • Canada • May 15-19 2017

# Elastic least-squares migration with two-way wave equation forward and adjoint operators

*Ke Chen and Mauricio D. Sacchi, Department of Physics, University of Alberta*

**Summary**

Time domain elastic least-squares reverse time migration (LSRTM) is formulated as a linearized elastic waveform inversion problem. The elastic Born approximation and elastic reverse time migration (RTM) operators are derived from the time-domain continuous adjoint-state method. We define P-wave and S-wave impedance perturbations as the unknown elastic images. The algorithm is obtained using a continuous functional form where the problem is discretized at the final state prior to applying quadratic optimization. The discretized numerical versions of the elastic Born and elastic RTM operators pass the dot product test. The conjugate gradients least-squares (CGLS) method is used to solve the least-squares migration optimization problem. The inverse of the diagonal of the Pseudo-Hessian operator is used to accelerate the convergence of the elastic LSRTM. The elastic LSRTM provides higher resolution images with fewer artifacts and a superior balance of amplitudes when compared to elastic RTM. More important, elastic LSRTM can remove cross-talk between the P-wave and S-wave impedance perturbations. Finally, we also show that the adopted Pseudo-Hessian preconditioning strategy accelerates convergence and improves the recovery of image amplitudes.

**Introduction**

Migration is the most commonly used tool to map the subsurface image in exploration seismology. Images obtained via migration suffer from relative low resolution, unbalanced amplitudes and artifacts. Different linearized inversion problems have been formulated to iteratively invert the migration blurring kernel: least-squares Kirchhoff migration (Tarantola, 1984; Nemeth et al., 1999), least-squares one-way wave equation migration (Kuehl and Sacchi, 2003; Wang et al., 2005; Kaplan et al., 2010) and least-squares reverse time migration (Bourgeois et al., 1989; Dai et al., 2012). The aforementioned LSM methods are based on acoustic approximation. Land data and ocean bottom data record both P- and S-waves and therefore, it is important to investigate least-squares migration for elastic media. Elastic least-squares ray-Born migration/inversion was implemented by Beydoun and Mendes (1989) and Jin et al. (1992) in heterogeneous medium. Anikiev et al. (2013) investigated the decoupling of parameters for frequency domain elastic LSRTM for the case of a point scatter in a homogeneous isotropic elastic background model. In these studies, the elastic parameter perturbations are inverted and used as “elastic images”. Stanton and Sacchi (2015) and Xu et al. (2016) utilized Helmholtz decomposition (Dellinger and Etgen, 1990) based wavefield separation for elastic least-squares split-step and reverse time migration for the inversion of elastic reflectivity volume in extended domain, respectively. In this article, a time-domain elastic LSRTM is formulated as a linearized elastic full waveform inversion problem (Chen and Sacchi, 2016). The elastic Born approximation and elastic RTM operators are derived via the adjoint-state method. The adjoint state equation system is the same with the state equation system with the only difference: the explosive source is replaced by adjoint source. In our work, P-wave and S-wave *impedance perturbations* are defined as elastic images. All derivations are in continuous functional form, the problem is discretized after developing the algorithm. The discretized numerical version of elastic Born approximation operator and elastic RTM operator pass the *dot product test* (Claerbout, 1992). The latter allows the use of conjugate gradient least-squares (CGLS) algorithm (Paige and Saunders, 1982) for solving the least-squares optimization problem. The inverse of the diagonal of the Pseudo-Hessian (Shin et al., 2001) is used to accelerate the convergence of the elastic LSRTM.

**Theory**

The propagation of seismic wave in isotropic elastic heterogeneous medium is governed by the equations

$$\begin{aligned} \rho\dot{\mathbf{v}} - \nabla\cdot\boldsymbol{\sigma} &= \mathbf{0}, \\ \dot{\boldsymbol{\sigma}} - \mu\left(\nabla\mathbf{v} + \nabla\mathbf{v}^T\right) - \lambda\left(\nabla\cdot\mathbf{v}\right)\mathbf{I} &= \mathbf{f}, \end{aligned} \tag{1}$$

where $\mathbf{v}$ denotes particle velocity field and $\sigma$ denotes the stress field, $\rho$ is the density, $\lambda$ and $\mu$ are the Lamé parameters, $\mathbf{f}$ is the explosive source term. The elastic wave equation is the state equation of the elastic parameter inversion problem when it is regarded as optimal control problem (Lions, 1971). The wavefield is a nonlinear implicit function of the model parameters

$$\mathbf{u} = \mathbf{u}(\mathbf{m}), \tag{2}$$

where $\mathbf{m} = (\rho, \lambda, \mu)^T$ and $\mathbf{u} = (\mathbf{v}, \sigma)^T$. A numerical method must be used to solve the forward problem. In this article, a time domain staggered-grid finite-difference scheme (Virieux, 1986) is utilized to discretize the continuous form elastic wave equation. The unsplit Convolutional Perfectly Matched Layer (C-PML) method is used to absorb the incident wave on the artificial boundaries (Komatitsch and Martin, 2007). Seismic migration techniques often rely on the adjoint

of the linearized forward problem. Taylor series expansion can be used for linearizing the nonlinear forward problem. We assume that the Lamé parameters are perturbed around a smooth background model $\lambda \rightarrow \lambda + \delta\lambda, \mu \rightarrow \mu + \delta\mu$. Dropping the second and higher order terms in the perturbed elastic wave equation leads to the following first-order Born approximation

$$\begin{aligned} &\rho\,\delta\dot{\mathbf{v}} - \nabla\cdot\delta\sigma = \mathbf{0}, \\ &\delta\dot{\sigma} - \mu(\nabla\delta\mathbf{v} + \nabla\delta\mathbf{v}^T) - \lambda(\nabla\cdot\delta\mathbf{v})\mathbf{I} = \delta\mu(\nabla\mathbf{v} + \nabla\mathbf{v}^T) + \delta\lambda(\nabla\cdot\mathbf{v})\mathbf{I}, \end{aligned} \tag{3}$$

where $\delta\mathbf{v}$ and $\delta\sigma$ are scattered particle velocity field and scattered stress field due to model perturbations $\delta\lambda$ and $\delta\mu$, $\mathbf{v}$ is the incident particle velocity field in the smoothed background model $\rho$, $\lambda$ and $\mu$. The right side of equation is the so-called "secondary source". The scattered wavefield can be computed using the same finite-difference codes that is adopted to compute the source side incident wavefield in equation 1. The relationship between the model perturbations and wavefield perturbations is linear (Born approximation)

$$\delta\mathbf{u} = \frac{\partial\mathbf{u}}{\partial\mathbf{m}}\delta\mathbf{m} = \mathscr{F}\delta\mathbf{m}, \tag{4}$$

where $\delta\mathbf{m} = (\delta\lambda, \delta\mu)^T$, $\delta\mathbf{u} = (\delta\mathbf{v}, \delta\sigma)^T$ and $\mathscr{F}$ is the Fréchet derivative. We denotes the Born modelling as follows

$$\delta\mathbf{d} = \mathscr{T}\delta\mathbf{u} = \mathscr{T}\mathscr{F}\delta\mathbf{m} = \mathscr{L}\delta\mathbf{m}, \tag{5}$$

where operator $\mathscr{T}$ represents the sampling of wavefield at receiver locations. The migration operator is the adjoint of the Born modelling operator that maps from reflection data to model perturbation or image

$$\delta\mathbf{m} = \mathscr{L}^\dagger\delta\mathbf{d} = \mathscr{F}^\dagger\mathscr{T}^\dagger\delta\mathbf{d}, \tag{6}$$

where $\mathscr{L}^\dagger$ is reverse time migration operator. After derivations using time domain continuous adjoint-state method (Lions, 1971; Fichtner et al., 2006), we obtain

$$\delta\lambda = \int_0^T (\nabla\cdot\mathbf{v})(\nabla\cdot\int_0^T \upsilon\mathrm{d}t)\mathrm{d}t, \quad \delta\mu = \int_0^T (\nabla\mathbf{v} + \nabla\mathbf{v}^T) : (\nabla\int_0^T \upsilon\mathrm{d}t)\mathrm{d}t, \tag{7}$$

with $\upsilon$ as adjoint-state particle velocity field that can be computed using the adjoint-state equation

$$\begin{aligned} \rho\,\dot{\upsilon} - \nabla\cdot\varsigma &= -\mathscr{T}^\dagger\delta\mathbf{d}, \\ \dot{\varsigma} - \mu\left(\nabla\upsilon + \nabla\upsilon^T\right) - \lambda\,(\nabla\cdot\upsilon)\,\mathbf{I} &= \mathbf{0}, \end{aligned} \tag{8}$$

where $-\mathscr{T}^\dagger\delta\mathbf{d}$ is the adjoint source. The same finite-difference code adopted to solve the forward equation system 1 and Born modelling equation system 3 can be reused to compute the adjoint wavefield in equation 8. The only difference is that the source term is replaced by the adjoint source and the finite-difference steps are in time reversal mode. A careful discretization of the aforementioned linear operators leads to a numerical forward elastic Born approximation operator $\mathscr{L}$ and a numerical elastic RTM operator $\mathscr{L}^\dagger$ pass the dot product test (Claerbout, 1992). The elastic least-squares reverse time migration is formulated as a quadratic optimization problem

$$\mathscr{J}(\delta\mathbf{m}) = \frac{1}{2}\sum_{i=1}^{N_s} \|\mathscr{L}_i\delta\mathbf{m} - \delta\mathbf{d}_i\|_2^2, \tag{9}$$

where $\mathscr{L}_i$ is the Born operator for the $i$th shot, $\delta\mathbf{d}_i$ is the reflection data associated to the $i$th shot gather, $\delta\mathbf{m}$ is the model perturbation (image) relative to the background model, $N_s$ indicates the number of shots. For reflection seismic data, P- and S-wave impedance are most suitable parameters for elastic waveform inversion (Tarantola, 1986). We parameterized our elastic LSRTM in terms of P-wave impedance perturbation $\delta I_p$ and S-wave impedance perturbation $\delta I_s$. Using the chain rule, the relationship between model perturbations can be written as follows

$$\begin{pmatrix} \delta I_p \\ \delta I_s \end{pmatrix} = \begin{pmatrix} 2V_p & 0 \\ -4V_s & 2V_s \end{pmatrix} \begin{pmatrix} \delta\lambda \\ \delta\mu \end{pmatrix}. \tag{10}$$

In our algorithm , we have incorporated the parameter transformation matrix and its adjoint into the CGLS solver. The change of parameters is similar to adding preconditioning to our system of equations. The information from the Hessian can precondition the linear system of equations. The Hessian for elastic LSRTM is $\mathscr{H} = \sum_{i=1}^{N_s}\mathscr{L}_i^\dagger\mathscr{L}_i$. The latter is extremely expensive to compute. Shin et al. (2001) proposed to neglect the receiver Green's function to save computation cost. Under this assumption, the Hessian can be simplified to the so-called "Pseudo-Hessian"

$$\begin{aligned} \mathscr{H}^{\lambda\lambda}_{pseudo}(\mathbf{x},\mathbf{x}') &= \sum_{i=1}^{N_s}\int (\nabla\cdot\mathbf{v}(\mathbf{x})\mathbf{I}) : (\nabla\cdot\mathbf{v}(\mathbf{x}')\mathbf{I})\mathrm{d}t, \\ \mathscr{H}^{\mu\mu}_{pseudo}(\mathbf{x},\mathbf{x}') &= \sum_{i=1}^{N_s}\int (\nabla\mathbf{v}(\mathbf{x}) + \nabla\mathbf{v}(\mathbf{x})^T) : (\nabla\mathbf{v}(\mathbf{x}') + \nabla\mathbf{v}(\mathbf{x}')^T)\mathrm{d}t. \end{aligned} \tag{11}$$

We use the diagonal of Pseudo-Hessian to precondition the elastic LSRTM problem. The preconditioned version of our elastic LSRTM minimizes

$$\mathscr{J}(\delta\tilde{\mathbf{m}}) = \frac{1}{2}\sum_{i=1}^{N_s} \|\mathscr{L}_i \mathscr{P}_H \mathscr{P}_T \delta\tilde{\mathbf{m}} - \delta\mathbf{d}_i\|_2^2, \tag{12}$$

where $\mathscr{P}_H$ denotes Pseudo-Hessian preconditioning, $\mathscr{P}_T$ denotes the adjoint of parameter transformation matrix in equation 10, $(\delta\lambda, \delta\mu)^T = \mathscr{P}_H \mathscr{P}_T \delta\tilde{\mathbf{m}}$ and $(\delta I_p, \delta I_s)^T = {\mathscr{P}_T}^{-1}(\delta\lambda, \delta\mu)^T$. Elastic LSRTM problem 12 is solved by the preconditioned conjugate gradient least squares (PCGLS) algorithm (Bjorck, 1996).

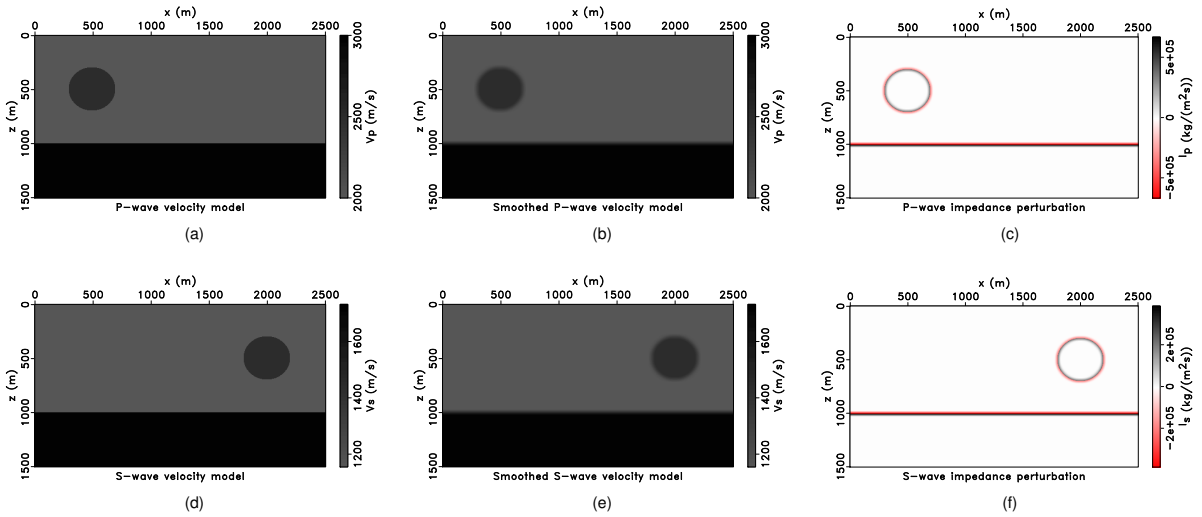


Figure 1: Elastic Camembert model. (a) Compressional velocity model. (b) Smoothed compressional velocity model. (c) True P-wave impedance perturbation. (d) Shear velocity model. (e) Smoothed shear velocity model. (f) True S-wave impedance perturbation.

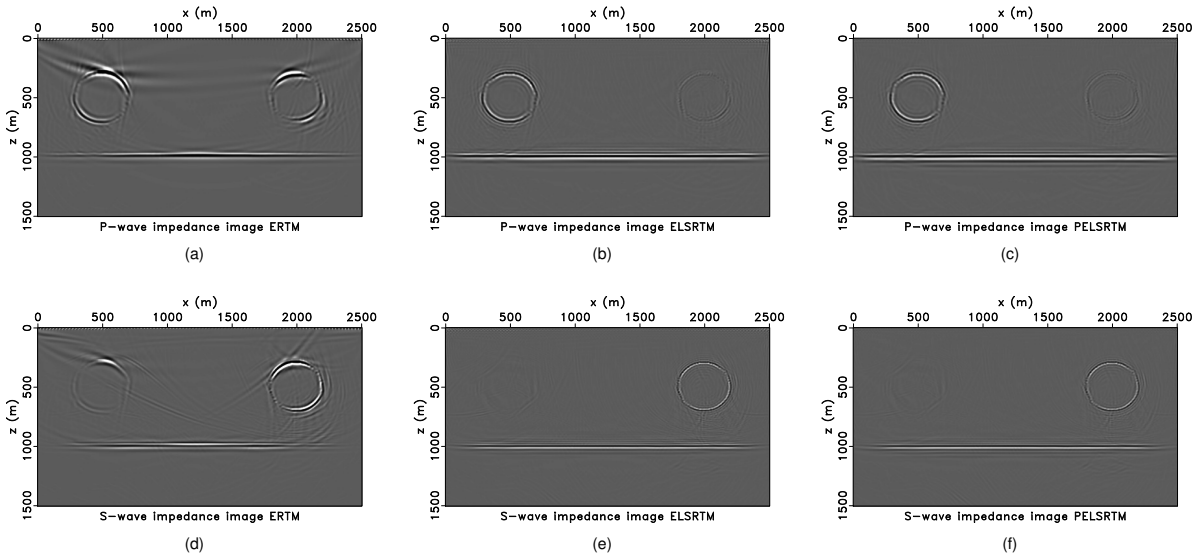


Figure 2: (a) P-wave impedance perturbation image got by elastic RTM. (b) P-wave impedance perturbation image got by elastic LSRTM. (c) P-wave impedance perturbation image got by preconditioned elastic LSRTM. (d) S-wave impedance perturbation got by elastic RTM. (e) S-wave impedance perturbation image got by elastic LSRTM. (f) S-wave impedance perturbation image got by preconditioned elastic LSRTM.

## Examples

The codes for our numerical examples were written in C and parallelized with Message Passing Interface (MPI). All the "observed data" in this article are generated with time-domain elastic finite-difference method. Figure 1 a and d show the true compressional and shear velocity models for the elastic Camembert model. The velocity anomalies for P and S

are in different positions. Density is assumed to be constant. Figure 1 b and e show the smoothed background velocity models for elastic RTM or elastic LSRTM. Figure 1 c and f show the true P-wave and S-wave impedance perturbations with respect to the background models. The results of elastic RTM (Figure 2 a and d) contain obvious cross-talk between P-wave and S-wave impedance perturbations and migration artifacts. Elastic LSRTM (Figure 2 b and e) not only can remove the multi-parameter cross-talk but also has fewer artifacts, more balanced amplitudes and higher resolution. The results were computed after $82$ iterations of the elastic LSRTM. The relative data misfit percentage reduces to $6\%$. Figure 2 c and f show the Pseudo-Hessian preconditioned elastic LSRTM after $35$ iterations.The relative data misfit also reduces to $6\%$. The results are similar with un-precondition elastic LSRTM. Figure 3 a and d shows the modified elastic Marmousi2 P- and S-wave velocity models. In the steep fault zone, there are two hydrocarbon reservoirs around depth $500$ m that have decreased P-wave velocity and a small change in the S-wave velocity. This uncorrelated P- and S-wave structure will cause cross-talk in elastic RTM images. Figure 3 b and e show the smoothed background velocity model for elastic RTM and elastic LSRTM. Figure 3 c and f show the true P-wave and S-wave impedance perturbation with respect to the smoothed background models. From this figure, we can also see that the P- and S-wave models are inconsistent in the two hydrocarbon reservoirs region at around $500$ m depth in the steep fault zone.

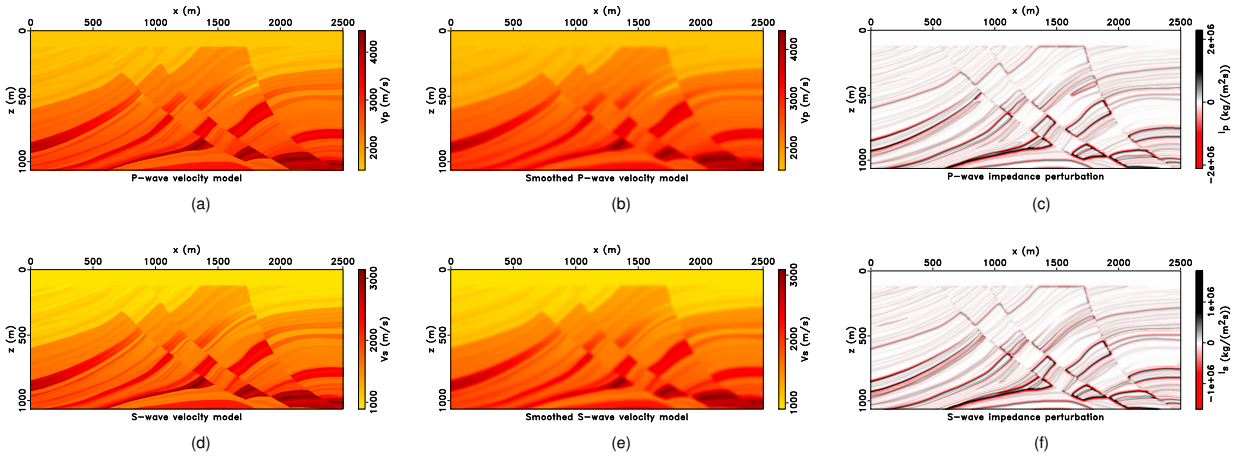


Figure 3: Elastic Marmousi2 model. (a) Compressional velocity model. (b) Smoothed compressional velocity model. (c)True P-wave impedance perturbation. (d) Shear velocity model. (e) Smoothed shear velocity model. (f) True S-wave impedance perturbation.

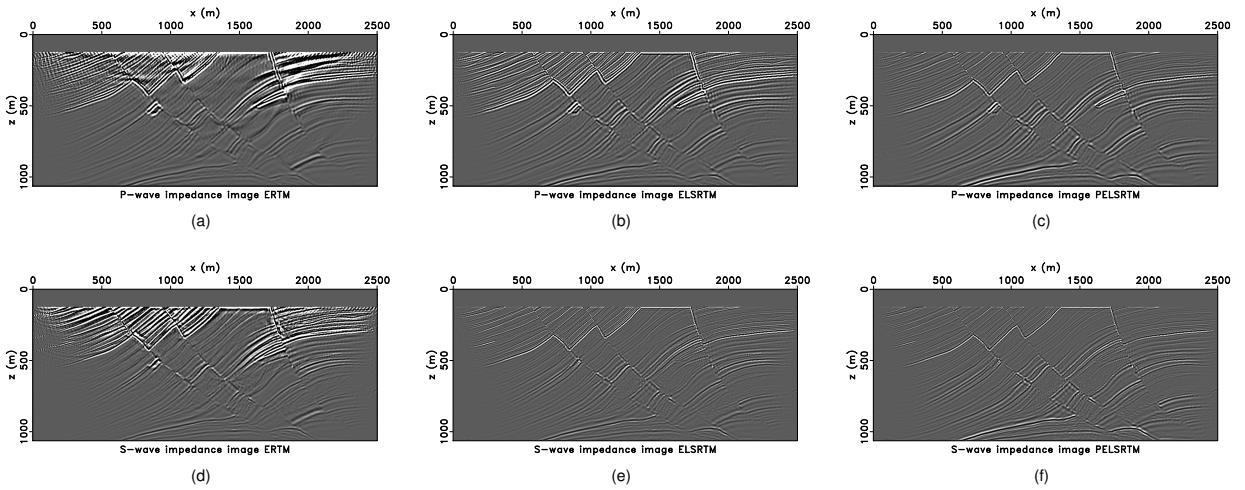


Figure 4: (a) P-wave impedance perturbation image got by elastic RTM. (b) P-wave impedance perturbation image got by elastic LSRTM. (c) P-wave impedance perturbation image got by preconditioned elastic LSRTM. (d) S-wave impedance perturbation got by elastic RTM. (e) S-wave impedance perturbation image got by elastic LSRTM. (f) S-wave impedance perturbation image got by preconditioned elastic LSRTM.

Figure 4 a and d show the P- and S- wave impedance perturbation images of elastic RTM. It successfully imaged most of the geology structures. However, the image amplitudes are unbalanced for shallow and deep parts of the model. Even though after applying Laplacian filter, the images still have high amplitude low frequency RTM artifacts. There

are also uncollapsed energy artifacts caused by not having a dense distribution of sources and limited aperture. Most important, the elastic RTM operator generated cross-talk between P and S images in the two hydrocarbon reservoir areas because the P- and S-wave velocity structure are different. The elastic LSRTM was iterated for $98$ iterations. The relative data misfit percentage reduces to $40\%$. The elastic LSRTM (Figure 4 b and e) corrected the unbalanced amplitudes and suppressed the low-frequency RTM artifacts and artifacts caused by limited aperture. The elastic LSRTM also generate higher-resolution images. More important, the elastic LSRTM can successfully decouple multi-parameters and suppress multi-parameter cross-talk in the hydrocarbon reservoir area in P and S images. Figure 4 c and f shows the Pseudo-Hessian preconditioned elastic LSRTM after $55$ iterations whose relative data misfit also reduces to $40\%$.

**Conclusions**

The elastic LSRTM produces higher resolution images with fewer artifacts and more balanced amplitudes than elastic RTM. More important, elastic LSRTM can remove the multi-parameter cross-talk that are presented in elastic RTM images. In essence, the off-diagonal elements of the Hessian operators are attenuated by the inversion process. The Pseudo-Hessian preconditioning operator adopted in our work not only accelerates convergence but also improves the amplitude response of our images.

**Acknowledgements**

We wish to thank the sponsors of the Signal Analysis and Imaging Group (SAIG) at the University of Alberta for financial support of this research. High-performance cluster computational resources were provided by WestGrid Compute Canada. The figures in this paper were plotted using the Madagascar open-source software package.

**REFERENCES**

Anikiev, D., B. Kashtan, and W. A. Mulder, 2013, Decoupling of elastic parameters with iterative linearized inversion: 83rd Annual International Meeting, SEG, Expanded Abstracts, 3185–3190.

Beydoun, W. B., and M. Mendes, 1989, Elastic ray-Born l2-migration/inversion: Geophysical Journal International, **97**, 151–160.

Bjorck, A., 1996, Numerical methods for least squares problems: Society for Industrial and Applied Mathematics.

Bourgeois, A., B. F. Jiang, and P. Lailly, 1989, Linearized inversion: a significant step beyond pre-stack migration: Geophysical Journal International, **99**, 435–445.

Chen, K., and M. D. Sacchi, 2016, Elastic least-squares reverse time migration via linearized elastic full waveform inversion with pseudo-hessian preconditioning: Signal Analysis and Imaging Group, Report 17, University of Alberta, 274–310.

Claerbout, J. F., 1992, Earth soundings analysis: Processing versus inversion: Blackwell Scientific Publications Cambridge, Massachusetts, USA, **6**.

Dai, W., P. Fowler, and G. T. Schuster, 2012, Multi-source least-squares reverse time migration: Geophysical Prospecting, **60**, 681–695.

Dellinger, J., and J. Etgen, 1990, Wavefield separation in two-dimensional anisotropic media: Geophysics, **55**, 914–919.

Fichtner, A., H.-P. Bunge, and H. Igel, 2006, The adjoint method in seismology: I. theory: Physics of the Earth and Planetary Interiors, **157**, 86 – 104.

Jin, S., R. Madariaga, J. Virieux, and G. Lambar, 1992, Two-dimensional asymptotic iterative elastic inversion: Geophysical Journal International, **108**, 575–588.

Kaplan, S. T., P. S. Routh, and M. D. Sacchi, 2010, Derivation of forward and adjoint operators for least-squares shot-profile split-step migration: Geophysics, **75**, S225–S235.

Komatitsch, D., and R. Martin, 2007, An unsplit convolutional perfectly matched layer improved at grazing incidence for the seismic wave equation: Geophysics, **72**, SM155–SM167.

Kuehl, H., and M. D. Sacchi, 2003, Least-squares wave-equation migration for AVP/AVA inversion: Geophysics, **68**, 262–273.

Lions, J. L., 1971, Optimal control of systems governed by partial differential equations: Springer Berlin Heidelberg.

Nemeth, T., C. Wu, and G. T. Schuster, 1999, Least-squares migration of incomplete reflection data: Geophysics, **64**, 208–221.

Paige, C. C., and M. A. Saunders, 1982, LSQR: An algorithm for sparse linear equations and sparse least squares: ACM Trans. Math. Softw., **8**, 43–71.

Shin, C., S. Jang, and D.-J. Min, 2001, Improved amplitude preservation for prestack depth migration by inverse scattering theory: Geophysical Prospecting, **49**, 592–606.

Stanton, A., and M. Sacchi, 2015, Least squares wave equation migration of elastic data: 77th Annual International Conference and Exhibition, EAGE, Extended Abstracts.

Tarantola, A., 1984, Linearized inversion of seismic reflection data: Geophysical Prospecting, **32**, 998–1015.

——, 1986, A strategy for nonlinear elastic inversion of seismic reflection data: Geophysics, **51**, 1893–1903.

Virieux, J., 1986, P-SV wave propagation in heterogeneous media: Velocity-stress finite-difference method: Geophysics, **51**, 889–901.

Wang, J., H. Kuehl, and M. D. Sacchi, 2005, High-resolution wave-equation ava imaging: Algorithm and tests with a data set from the western canadian sedimentary basin: Geophysics, **70**, S91–S99.

Xu, L., A. Stanton, and M. Sacchi, 2016, Elastic least-squares reverse time migration: 86th Annual International Meeting, SEG, Expanded Abstracts, 2289–2293.